J|A|C|S ARTICLES

Published on Web 01/27/2009

Effects of Lattice Expansion on the Reactivity of a One-Dimensional Oxide

Cristina Africh,*[,†,‡] Lukas Köhler,[§] Friedrich Esch,[‡] Martina Corso,[⊥,†,‡] Carlo Dri,[†,‡] Tomas Bucko,[§] Georg Kresse,[§] and Giovanni Comelli[†,‡]

Physics Department and Center of Excellence for Nanostructured Materials, University of Trieste, I-34127 Trieste, Italy, CNR-INFM TASC Laboratory, I-34012 Basovizza, Trieste, Italy, and Faculty of Physics and Center for Computational Materials Science, University of Vienna, Sensengasse 8/12, 1090 Vienna, Austria

Received October 14, 2008; E-mail: africh@tasc.infm.it

Abstract: By means of scanning tunneling microscopy (STM) and density functional theory (DFT) calculations, we characterize at the single-atom level the mechanism of the water formation reaction on the (10 × 2)-O/Rh(110) surface, a prototype of a one-dimensional (1D) oxide where the lattice expansion and the segmentation of the surface play a fundamental role. When the reaction is imaged in the 238−263 K temperature range (35 s/image acquisition time), a peculiar comblike propagation mechanism for the reaction front is found. Fast STM measurements (33 ms/image) prove that this mechanism holds also at room temperature, being therefore an intrinsic characteristic of the reaction on the 1D oxide. DFT calculations explain the observed behavior as due to the interplay between the lattice expansion in the initial surface and its relaxation during the reaction that leads to varying configurations for the reactants. At low temperatures, the reaction produces, in its final stages, a low-coverage, ordered patterning of the surface with residual oxygen. The pattern formation is related to the segmentation of the oxide phase.

Introduction

In recent years, the formation and reactivity of surface oxides have received a growing interest within the surface science community.[1,2] One-dimensional (1D) stripes, two-dimensional layers, or three-dimensional thin films of metal oxides have proven to form on late transition metals (TM) by exposure to an oxidizing atmosphere. These oxides might play a fundamental role in catalysis under real operation conditions.[3,4] 1D oxides with very similar metal/oxygen configurations (one metal atom coordinated to four O atoms) were found on Pt and Rh surfaces, both on flat terraces[5−9] and at steps on vicinal surfaces.[10,11] On Pt(110), such structures turned out to be extremely active for CO oxidation in DFT calculations.[5,10] Indeed, a commensurate oxide composed of 1D metal/oxygen stripes (possibly stabilized by the presence of carbonate ions) was found as a highly reactive intermediate phase during catalytic CO oxidation on Pt(110) in a flow reactor.[12] TM nanoparticles, which are commonly used in real catalysts, offer a wealth of defects (e.g., steps) that may easily undergo 1D oxidation under operating conditions.[13,14] A thorough study of 1D oxide reactivity is therefore crucial for the understanding of the nanoparticle reactivity under oxidizing conditions. All 1D oxides found on TM surfaces such as Rh(110)[8,9] and Pt(110)[5−7] as well as on vicinal Rh surfaces[11] are characterized by an in-plane expansion of the first metal layer along the close-packed direction, resulting in a segmentation of the surface. The issue we address here is how these segments and the relaxation within the segments influence the reactivity of the surface, leading to peculiar, comblike wave fronts and to adsorbate nanopatterning of the surface.

On Rh(110), in particular, an oxygen-induced structure with (10 × 2) periodicity forms on the (1 × 2) reconstructed

† University of Trieste.
‡ CNR-INFM TASC Laboratory.
§ University of Vienna.
⊥ Current address: Donostia International Physics Center (DIPC), 20018 Donostia-San Sebastian, Spain.

(1) Lundgren, E.; Mikkelsen, A.; Andersen, J. N.; Kresse, G.; Schmid, M.; Varga, P. *J. Phys.: Condens. Matter* **2006**, *18*, R481 and references therein.
(2) Reuter, K.; Scheffler, M. *Appl. Phys., A* **2004**, *78*, 793 and references therein.
(3) Hendriksen, B. L. M.; Bobaru, S. C.; Frenken, J. W. M. *Catal. Today* **2005**, *105*, 234.
(4) Nolte, P.; Stierle, A.; Jin-Phillipp, N, Y; Kasper, N.; Schulli, T. U.; Dosch, H. *Science* **2008**, *321*, 1654.
(5) Pedersen, T. M.; Li, W. X.; Hammer, B. *Phys. Chem. Chem. Phys.* **2006**, *8*, 1566.
(6) Li, W. X.; Österlund, L.; Vestergaard, E. K.; Vang, R. T.; Matthiesen, J.; Pedersen, T. M.; Lægsgaard, E.; Hammer, B.; Besenbacher, F. *Phys. Rev. Lett.* **2004**, *93*, 146104.
(7) Helveg, S.; Li, W. X.; Bartelt, N. C.; Horch, S.; Lægsgaard, E.; Hammer, B.; Besenbacher, F. *Phys. Rev. Lett.* **2007**, *98*, 115501.
(8) Vesselli, E.; Africh, C.; Baraldi, A.; Comelli, G.; Esch, F.; Rosei, R. *J. Chem. Phys.* **2001**, *114*, 4221.
(9) Africh, C.; Esch, F.; Li, W. X.; Corso, M.; Hammer, B.; Rosei, R.; Comelli, G. *Phys. Rev. Lett.* **2004**, *93*, 126104.
(10) Wang, J. G.; Li, W. X.; Borg, M.; Gustafson, J.; Mikkelsen, A.; Pedersen, T. M.; Lundgren, E.; Weissenrieder, J.; Klikovits, J.; Schmid, M.; Hammer, B.; Andersen, J. N. *Phys. Rev. Lett.* **2005**, *95*, 256102.
(11) Gustafson, J.; Resta, A.; Mikkelsen, A.; Westerström, R.; Andersen, J. N.; Lundgren, E.; Weissenrieder, J.; Schmid, M.; Varga, P.; Kasper, N.; Torrelles, X.; Ferrer, S.; Mittendorfer, F.; Kresse, G. *Phys. Rev. B* **2006**, *74*, 035401.
(12) Ackermann, M. D.; Pedersen, T. M.; Hendriksen, B. L. M.; Robach, O.; Bobaru, S. C.; Popa, I.; Quiros, C.; Kim, H.; Hammer, B.; Ferrer, S.; Frenken, J. W. M. *Phys. Rev. Lett.* **2005**, *95*, 255505.
(13) Mittendorfer, F.; Seriani, N.; Dubay, O.; Kresse, G. *Phys. Rev. B* **2007**, *76*, 233413.
(14) Li, W.-X. *J. Phys.: Condens. Matter* **2008**, *20*, 184022.

 © 2009 American Chemical Society

substrate.[8,9] The oxygen atoms adsorb on both sides of the top layer metal rows with a total coverage of almost two oxygen atoms per ridge Rh atom. The high local oxygen coverage leads to a lattice expansion of the topmost metal rows of about 11% in the [1$\bar{1}$0] direction. As a consequence, two out of ten Rh atoms are ejected, leaving segmented chains of eight Rh atoms, which are separated by ridge vacancies (RV) aligned in the [001] direction. The ejected metal atoms form unreconstructed areas, covered by adsorbed oxygen atoms, which coexist on the surface with the 1D oxide.

In a previous scanning tunneling microscopy (STM) and density functional theory (DFT) study,[9] we investigated at room temperature (RT) the water formation reaction taking place when the (10 × 2) surface is exposed to molecular hydrogen. We showed that this reaction proceeds in two steps: in the first step, a reaction front consumes half of the oxygen, leaving the remaining oxygen atoms in a zigzag pattern. The wave front crosses the surface rapidly, regardless of the local topography, i.e., regardless of the presence of an RV or the position of the specific ridge Rh atom with respect to the substrate. At the passage of the reaction front, the previously expanded Rh segments contract back to the Rh surface lattice constant. In the second reaction step, the remaining oxygen atoms are removed by a different reaction mechanism, starting from the now enlarged RVs, which are active sites for both H_2 dissociation and OH formation. Since the reaction can start from any RV, a reaction front is not observed here. In ref 9 we also demonstrated how the presence (removal) of the lattice expansion in the segments hides (exposes) active sites and thus steers the reactivity during the water formation reaction.

In this paper, we present new, detailed STM measurements, taken below room temperature, and new DFT calculations on the reaction studied at the single-atom level. We show that the reactivity of the oxygen in the 1D oxide is driven by the different registry of the Rh atoms in the expanded segments with respect to the underlying substrate, affecting both the thermodynamics and the kinetics as the water formation reaction proceeds along the segments. We also demonstrate how the nanostructuring of the initial surface, due to the lattice expansion and in particular to the regular segmentation, determines, after the low-temperature reaction, a low-coverage, ordered patterning of the surface with residual oxygen.

Experimental and Computational Methods

The experiments were performed in a UHV system (base pressure 1×10^{-10} mbar) equipped with standard sample preparation facilities and with an Omicron VT-STM. The (10 × 2) surface was prepared as described in ref 9. A series of STM images were acquired (typical scanning parameters: $I = 0.6-1$ nA, $V_b = +0.4$ to +0.6 V, 35 s/image) during exposure of the (10 × 2) surface to 1×10^{-8} mbar of molecular hydrogen (pressure corrected for the tip screening factor value as estimated in ref 15) at temperatures in the 238−263 K range.

The ab initio calculations were performed using the Vienna Ab Initio Simulation Package (VASP)[16] with the projector augmented wave method[17] in the implementation of Kresse and Joubert.[18] A plane wave cutoff of 250 eV was used, and the Generalized Gradient Approximation (GGA)[19] was applied throughout this work. The Brillouin zone integration was performed using a grid of (1 × 4) *k*-points in the (10 × 2) unit cell. The Rh substrate was described by a six-layer thick slab. The bottom two layers were fixed, whereas the top four layers were allowed to relax (asymmetric setup). Simulated STM images were obtained using the Tersoff-Hamann approach,[20] simulating tunneling from the tip toward empty states between 0.6 and 0.0 eV.

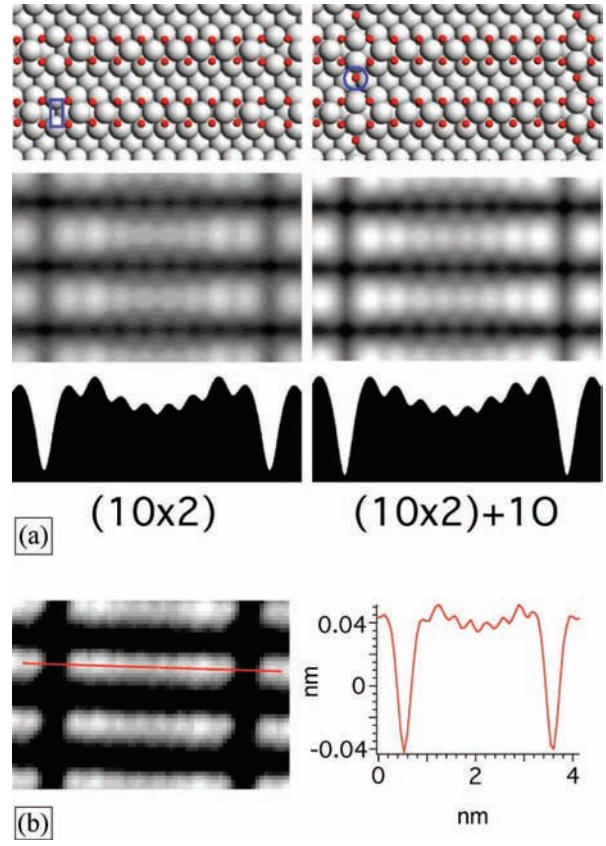

Figure 1. Structural model of the 1D oxide on Rh(110). (a) Model (top), simulated STM image (middle), and line profile across the simulated image (bottom) of the (10 × 2) (left) and the (10 × 2)+1O (right) structures. The rectangle in the model on the left and the circle in the model on the right indicate a ridge vacancy (RV) and the added oxygen, respectively. (b) Experimental STM image and height profile across the indicated line. (4.5 × 3.1 nm^2; $I = 0.6$ nA; $V_b = +0.6$ V.)

Results

Structural Analysis. The basic structural features of the Rh(110)-(10 × 2)-O surface are well-established and have already been elaborated in the Introduction. Two very similar structural models that differ only by the presence of one additional oxygen atom at the RV have been proposed in earlier studies: in our previous investigation of the reactivity of the surface upon hydrogen exposure,[9] we considered 18 O atoms per (10 × 2) unit cell, placed symmetrically on the Rh segments (see Figure 1a, left). However, in a more recent study, it was demonstrated that a slightly different model is thermodynamically more stable.[21] This model contains 19 O atoms per (10 × 2) unit cell, where the additional oxygen is located in the Rh channels at the RVs (see Figure 1a, right).

(15) Africh, C.; Esch, F.; Comelli, G.; Rosei, R. *J. Chem. Phys.* **2001**, *115*, 477.
(16) Kresse, G.; Furthmüller, J. *Comput. Mater. Sci.* **1996**, *6*, 15.
(17) Blöchl, P. E. *Phys. Rev. B* **1994**, *50*, 17953.
(18) Kresse, G.; Joubert, D. *Phys. Rev. B* **1998**, *59*, 1758.
(19) Perdew, J. P.; Chevary, J. A.; Vosko, S. H.; Jackson, K. A.; Pederson, M. R.; Singh, D. J.; Fiolhais, C. *Phys. Rev. B* **1992**, *46*, 6671.
(20) Tersoff, J.; Hamann, D. R. *Phys. Rev. B* **1985**, *31*, 805.
(21) Dri, C.; Africh, C.; Esch, F.; Comelli, G.; Dubay, O.; Köhler, L.; Mittendorfer, F.; Kresse, G.; Dudin, P.; Kiskinova, M. *J. Chem. Phys.* **2006**, *125*, 094701.

The simulated STM images of these structures are very similar (see Figure 1a) and can be distinguished only by the brightness of the outermost Rh atoms, which appear higher in the thermodynamically more stable (10 × 2)+1O model. However, in the experimental STM images a line profile that corresponds to the less stable (10 × 2) model is usually observed (see Figure 1b). Line profiles with brighter outermost atoms are also found, but only with either particularly low or oxygen-enriched background pressures. The difference between theory and experiment can most likely be attributed to the reaction with background gases. In fact, our calculations show that the additional oxygen atom is significantly more weakly bound than any oxygen atom along the Rh segments (−1.3 eV compared to values in the −2.1 to −2.4 eV range), and is thus easily reacted off, converting the (10 × 2)+1O into the (10 × 2). For this reason, it is not expected that the presence of the additional oxygen atom influences the reaction mechanism significantly.

First Reaction Step. At the temperatures used in the present study (238−263 K), the water formation reaction is slow enough to be studied by STM with unprecedented detail. The two-step mechanism already found at RT[9] is confirmed but peculiar additional features are found.

As reported in the Introduction, in the first reaction step, half of the oxygen atoms are removed by a reaction front, leaving the remaining O atoms in a zigzag pattern. The sequence of images reported in Figure 2 reveals the propagation mechanism of the wave front at 253 K. The reaction enters the imaged area from the one layer deep unreconstructed pit indicated by the big yellow arrow in Figure 2a. From the pit it propagates to one of the neighboring RVs and proceeds along the [001] oriented RV channel (see red arrows in Figure 2a,b), expanding onto the adjacent segments. As illustrated in the model in Figure 2e, at these low temperatures only one-half of each segment is reduced and the reaction front rapidly propagates along the RVs. The second half of each segment remains fully oxygen-covered, until it is reached by the reaction front attacking the segment from the other side (also see Figure 2c,d). Consequently, the reaction front takes on a comblike shape, with the "handle" along the RV channel and many orthogonal "teeth" on the adjacent segments. Figure 2f shows a zoom on such segments and clearly demonstrates that the reaction stops in the middle of each segment. The upper halves of the segments in the middle of the image have already participated in the reaction and only half of the original oxygen atoms are still present, arranged in a zigzag pattern. The lower halves of the segments are still unreacted and all the original oxygen atoms are present. The length of the unreacted part (the propagation length) cannot be determined accurately from the STM images. Indeed, the simulated images in Figure 1g show that there is only a tiny difference in the appearance of segments where 4 (left) or 5 (right) oxygen atoms are removed. However, the propagation length appears not to appreciably vary in the temperature range where the comblike mechanism can be tracked.

The appearance of a comblike reaction front is a new feature with respect to the behavior at RT, where the reaction front was seen to cross uniformly the surface, without being influenced by the presence of the RVs and of the lattice expansion.[9] When the temperature is lowered from 273 K, where only a uniform front is observed, progressively more areas with comblike fronts become visible, becoming dominant at around 260 K. At 238 K only comblike fronts are observed. This experimental observation does not necessarily imply a different behavior of the reaction at different temperatures. The uniform

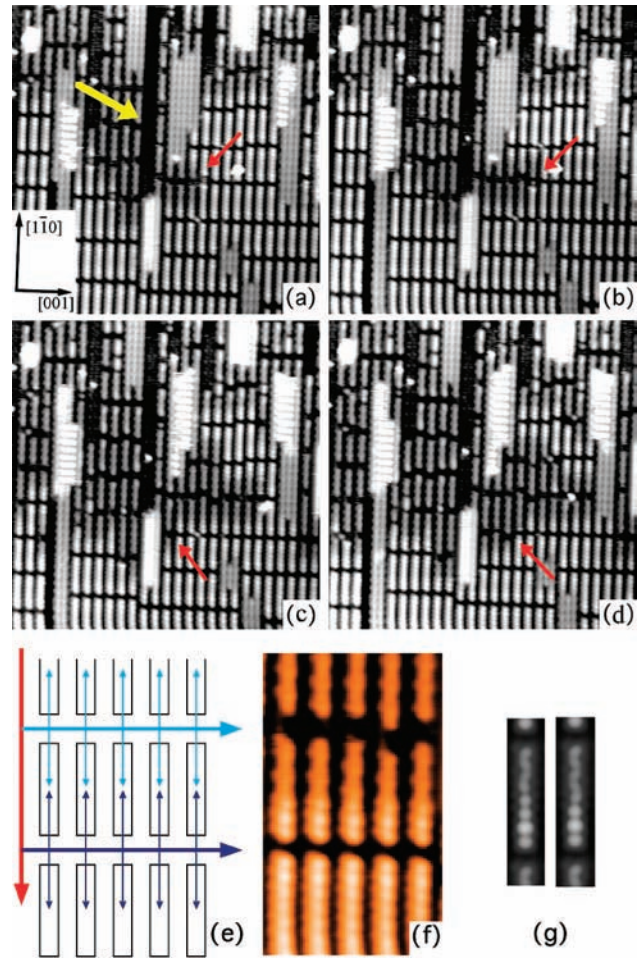

Figure 2. Comblike reaction front in the first reaction step at 253 K. (a−d) Sequence of STM images. The reaction enters the imaged area from the pit indicated by the big yellow arrow. On the segments, reacted regions appear darker. The small red arrows indicate the position of the front, proceeding along an RV channel (a,b) and then involving an adjacent RV channel (c,d) [26 × 26 nm^2; I = 0.6 nA; V_b = +0.6 V; time span between (a) and (b) 35 s; between (b) and (c) 3 min; between (c) and (d) 35 s]. (e) Schematic picture of the comblike propagation mechanism. The main propagation direction is indicated in red. From this main branch the reaction first proceeds along the upper RV channel following the light blue path and then along the lower RV channel following the dark blue path. (f) STM image of a 3.0 × 4.3 nm^2 area of the surface immediately after the passage of the reaction front in the upper channel (corresponding to the light blue path in (e)). On the reacted part, the zigzag due to the remaining O atoms is clearly visible. (g) Simulated STM images of a segment where 4 (left) or 5 (right) oxygen atoms are removed.

appearance of the reaction front at higher temperatures might be caused simply by the used image acquisition rate (typically 20 s/image). To clarify this point, we repeated the experiment at RT by monitoring the reaction with our Fast-STM Module,[22] which allows about 2 orders of magnitude faster image acquisition rates. We found indeed a local comblike propagation of the reaction front also at this temperature but on a much faster time scale. Figure 3 shows three snapshots of an STM movie acquired at RT with 33 ms/image acquisition time. An RV channel is highlighted in the lower part of the first image. Despite the reduced resolution (70 × 70 pixels), which makes it impossible to resolve individual atoms in the images, it is apparent that the lower part of the upper segments is brighter than their upper part, indicating the presence of unreacted Rh

(22) Esch, F.; Spessot, A.; Dri, C.; Africh, C.; Cornelli, G. In preparation.

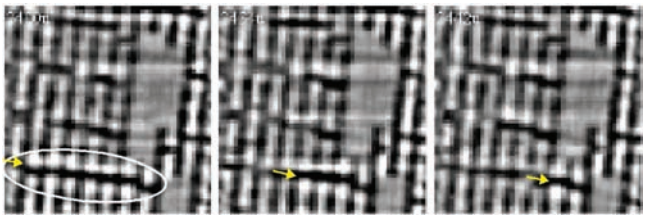

Figure 3. Snapshots from a Fast-STM movie of the reaction at RT. An RV channel is highlighted in the first image. The arrows indicate the propagation of the reaction along the channel. [82 × 113 Å^2; $I = 3$ nA; $V_b = +0.4$ V; fast scanning frequency (x direction), 2.13 kHz; image frequency, 30 Hz; time span between first and second image, 2244 ms; time span between second and third image, 528 ms.]

atoms and thus implying that the reaction stops somewhere in the middle of these segments. The second and the third image show the propagation of the wavefront along the RV channel (see arrows), similarly to what was evidenced at lower temperatures. It is clear, therefore, that the comblike mechanism is an intrinsic feature of the water formation reaction on the (10 × 2) surface, although at low temperature the propagation of the reaction front from one RV to the next (and therefore the comblike mechanism) is further facilitated by the reduced mobility of the metal atoms. As we discussed in our previous work,[9] in fact, the passage of the reaction front leads also to the diffusion of Rh atoms between subsequent segments in the [1$\bar{1}$0] direction. This transient mobility decreases dramatically when the temperature is decreased. At room temperature, the reaction front leaves behind a disordered surface where the RVs (and therefore the RV channels for the propagation of the reaction) are no longer aligned.[9] In the temperature range used for the present study, conversely, the Rh segments remain almost aligned, since only the outermost Rh atom, next to the RV, is able to move.

To understand the reason for the observed peculiar stopping of the reaction in the middle of the segments, we resort to DFT calculations. The capability of the VASP code to handle large unit cells, and hence an entire (10 × 2) unit cell, gives us the possibility to precisely elucidate the reaction mechanism atom by atom, obtaining a much better description than that in our previous study, where models with (6 × 2) periodicity were used to mimic different parts of the segments.

For the calculations, we always assume that the observed O removal reaction proceeds in two steps. As shown in the scheme of Figure 4, first the oxygen atoms are hydrogenated, and subsequently the OH diffuses away from the chain, moving into the missing row trough and then diffusing along it, until it reacts with a second hydrogen atom to form water. While both barriers for reaching the trough and diffusing along it are rather small ($E_{D1} = 0.2$ eV and $E_{D2} = 0.4$ eV, respectively), the first hydrogenation step involves markedly larger barriers of about 0.8 eV (see below). We therefore concentrate our detailed analysis to OH formation, which is the rate-limiting step. Furthermore, since the barrier for hydrogenation is largely determined by the stability of the OH group, we will first concentrate on the OH formation energies (E_{OH}), as defined in Figure 4.

First of all, we confirm the previous finding that oxygen removal is initially most favorable at the RVs.[9] The OH formation energy E_{OH} on an unreacted segment, where all O atoms are still present, is in fact largest at the end of the segment (1st O, −0.55 eV), and decreases for O atoms closer to the middle of the segment: −0.45 eV (2nd O), −0.36 eV (3rd O),

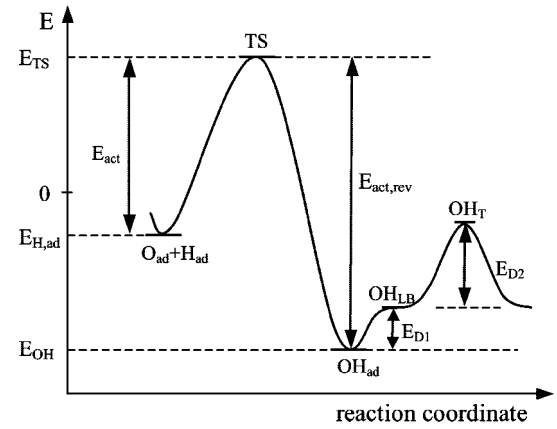

Figure 4. Sketch of the energetics of the OH formation reaction and subsequent diffusion. $E_{H,ads}$, E_{OH}, and E_{TS} are the hydrogen adsorption, OH formation, and transition state energies, respectively. E_{act} is the activation energy (barrier) for the formation reaction. $E_{act,rev}$ is the activation energy for the *reverse* reaction. OH_{ad} refers to OH adsorbed at the ridge sites and OH_{LB} and OH_T to OH adsorbed in the trough, in second layer long bridge and third layer on top sites, respectively. E_{D1} and E_{D2} are the OH barriers for moving to the trough and diffusing along it. The energy zero is the total energy of the starting oxygen adsorption structure + $^1/_2$ free H_2 molecule.

−0.33 eV (4th O), and −0.31 eV (5th O), thus confirming that the hydrogenation reaction starts from the RV and not in the middle of a segment.

Turning now to the propagation of the reaction, we modeled it by progressively removing oxygen atoms from the ridges. We first consider pure thermodynamic arguments. The adsorption geometry of the OH group in three different selected positions along the segment is shown in Figure 5a−c. It can be noted that the hydrogenation of the first O atom leads to a peculiar geometry, while the geometries for the OH groups in Figure 5b,c are essentially identical. The same holds for the adsorption geometries of the remaining OH groups, which are not shown. In general, the hydrogenation of O atoms within the segments leads also to a change of the distance between the adjacent ridge Rh atoms, as summarized in Table 1 together with the OH formation energies. Clearly, E_{OH} strongly varies as the reaction proceeds. The reason for this variation can be found in the relaxation of the Rh atoms in the segment. The interaction between the Rh chain and the OH group is significantly weaker than the interaction between the Rh chain and the oxygen atom. Therefore, OH formation usually leads to a relaxation of the neighboring ridge Rh atoms toward each other with a net energy gain. The magnitude of this relaxation correlates with E_{OH}. It can be seen that E_{OH} is largest for the third OH group (−0.91 eV), when also the relaxation is largest, whereas for the OH formation reaction #6 no relaxation occurs and, as a result, E_{OH} is the smallest (−0.59 eV), comparable to E_{OH} for the first OH group, when no relaxation is possible because there is only one adjacent Rh ridge atom. The formation of the second OH group is special since the Rh−Rh distance increases, but even in this case the relaxation leads to an energy gain. The increased Rh−Rh distance leads to a displacement of the outermost Rh atom toward the RV. This can facilitate the detachment of this atom from the segment to join the adjacent segment on the other side of the RV. Indeed, as described above, the outermost Rh atoms are the only ones that are experimentally observed to cross the RV already at low temperature at the passage of the reaction.

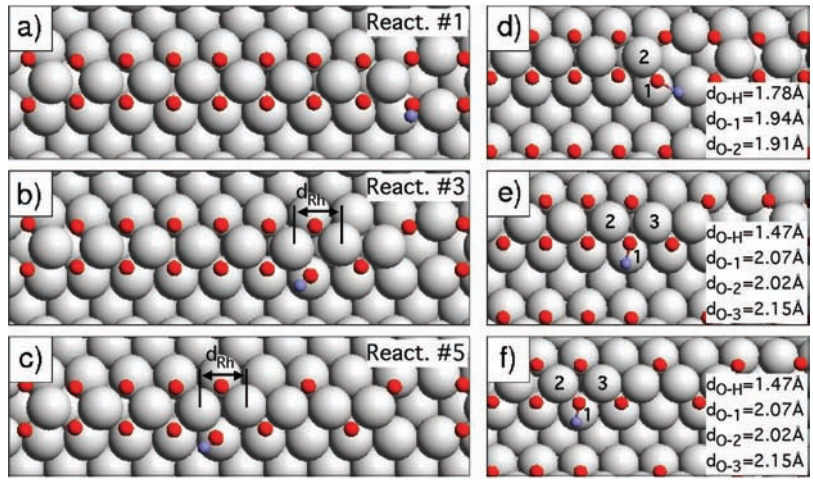

Figure 5. Modeling of the first reaction step. (a−c): Adsorption geometries of OH group if zero (a), two (b), and four (c) oxygen atoms have been removed. (d−f): Transition state geometries for the first (d), third (e), and fifth (f) OH formation reaction. Values of the distance of the O atom to the H atom and the neighboring Rh atoms are indicated. Rh atoms are drawn in gray, oxygen atoms in red, and hydrogen atoms in blue.

Table 1. Calculated Distances d_{Rh} between the Two Ridge Rh Atoms Adjacent to the OH Group before and after OH Formation[a]

reaction #	d_{Rh} without OH (Å)	d_{Rh} with OH (Å)	Δd_{Rh} (Å)	E_{OH} (eV)
1				−0.55
2	3.097	3.280	−0.183	−0.76
3	3.110	2.720	0.390	−0.91
4	2.912	2.771	0.141	−0.72
5	2.941	2.848	0.093	−0.67
6	3.009	3.017	−0.008	−0.59

[a] The Rh−Rh distance variation (Δd_{Rh}) upon OH formation is also reported. The OH formation energies E_{OH} are given with respect to $^1/_2$ free H_2 molecule: $E_{OH} = E_{slab/(n-1)O+OH} - E_{slab/nO} - {}^1/_2E_{H2}$.

Table 2. Calculated Energetics for OH Formation on the (10 × 2) Structure (See Diagram in Figure 4)[a]

reaction #	$E_{H,ad}$ (eV)	E_{TS} (eV)	E_{OH} (eV)	E_{act} (eV)	$E_{act,rev}$ (eV)
1	−0.29	0.50	−0.55	0.79	1.05
2	−0.13	(0.58)	−0.76	(0.71)	(1.34)
3	−0.19	0.47	−0.91	0.66	1.38
4	−0.22	(0.62)	−0.72	(0.84)	(1.34)
5	−0.31	0.63	−0.67	0.94	1.30
6	−0.24	(0.75)	−0.59	(0.99)	(1.34)

[a] $E_{H,ad}$ is the adsorption energy of a H atom in the channels, E_{TS} is the energy of the transition state, E_{OH} is the OH formation energy, E_{act} is the activation energy (barrier) defined as $E_{act} = E_{TS} - E_{H,ad}$, $E_{act,rev}$ is the activation energy of the reverse reaction defined as $E_{act,rev} = E_{TS} - E_{OH}$. All energies are given with respect to $^1/_2$ isolated H_2 molecule. Values in parentheses are not derived from full DFT calculations but are estimated (see text).

Considering the trend of the OH formation energies in Table 1, it can be seen that E_{OH} is largest for the OH formation reaction #3 and decreases monotonically thereafter. This trend is already an indication that the reaction will become less favorable when moving toward the middle of the segment, although it does not explain the experimental observation that the reaction actually stops in the middle of the segments. Hence, we have to resort to kinetic arguments and to a careful study of the reaction barriers (E_{act}) shown in Figure 4. We started by calculating the transition state energy (E_{TS}) for three selected OH formation reactions (#1, #3, and #5). The geometries of the transition states are shown in Figure 5d−f, and the corresponding energies can be found in Table 2. It can be seen that, among the calculated barriers, E_{act} becomes the smallest for the OH formation reaction #3, whereas it is largest for reaction #5. When comparing the calculated geometries of the transition states for reactions #3 and #5, it is immediately obvious that the geometries are identical within the accuracy of the calculations, which yield in both cases an O−H distance of 1.47 Å and Rh−O distances of 2.07 Å to the Rh atom below the oxygen, 2.02 Å to the Rh atom at the fully oxygen-covered side of the segment, and 2.15 Å to the Rh atom on the reacted side of the segment. The transition state geometry for the first OH formation reaction, conversely, is different, with the O−H distance increased to 1.78 Å, and the Rh−O distances at 1.94 and 1.91 Å, respectively. As reported above, the geometries of the final states of the OH formation reactions #3 and #5 are also found to be almost identical, thus it can be expected that the reaction path and, consequently, the energetics from the transition state to OH adsorption should be very similar as well. Indeed, it is found that the *reverse* activation energies from OH to the transition state differ only by 0.08 eV (see Table 2). This indicates a late transition state, which is geometrically and energetically dominated by the final state (adsorbed OH). This allows us to estimate the absolute transition state energy (E_{TS}) for the OH formation reactions #2, #4, and #6 by simply adding 1.34 eV (average of the calculated reverse barrier for reactions #3 and #5) to the energy of the final state E_{OH} (see again the schematic diagram in Figure 4). From the values reported in Table 2, one immediately recognizes that E_{TS} increases substantially toward the middle of the segment.

To evaluate the variation in the *activation* energies of the OH formation reaction throughout the whole sequence (from reaction #1 to reaction #6), it is necessary to consider also the energetics of the initial (H adsorption) states of the reactions. Hydrogen is only very weakly adsorbed at the entry of the channels with a shallow adsorption energy of −0.13 eV with respect to H_2 before reaction #3. The H adsorption energy increases to −0.31 eV in the middle of the channel. Consequently, the trend we evidenced for the variation of E_{TS} when moving toward the center of the segments is further enhanced for E_{act}, becoming clearly larger after reaction #3. Removal of the sixth atom involves already an activation energy of 0.99 eV, whereas restarting the reaction from the other side of the segment involves a barrier of only 0.79 eV. At room temperature this energy difference corresponds to a difference in the reaction speed by a factor of $\exp(-200\ \text{meV}/k_BT)$, i.e., ∼2300, clearly

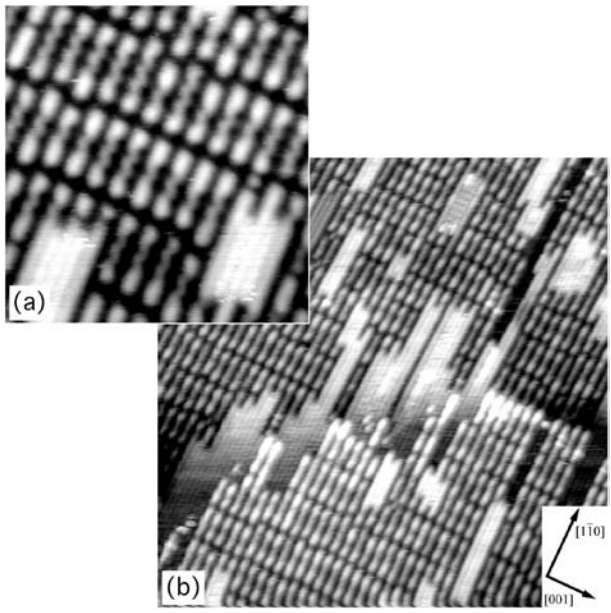

Figure 6. Oxygen nanopatterning in the second reaction step at 238 K. Reacted, oxygen-free parts appear brighter. (a) Short-range order (12 × 12.5 nm^2; I = 0.7 nA; V_b = +0.6 V; 285 min of H_2 exposure). (b) Long-range order (40 × 40 nm^2; I = 0.7 nA; V_b = +0.6 V; 244 min of H_2 exposure).

indicating that the reaction will stop after the fourth or fifth oxygen atom and then restart from the other side, in qualitative agreement with the experimental observation.

As described above, in this picture an important role is played by the H adsorption energy ($E_{H,ad}$) in the initial state. The variation of $E_{H,ad}$ can be traced back to the different geometries of O + H adsorption when moving along the segment. The interplay between the different registry of the O atoms along the segments with respect to the second surface layer and the partial removal of the lattice expansion, while the reaction proceeds, leads to an increased O−H distance of 2.73 Å in the initial state of reaction #5 compared to 2.64 Å for reaction #3. The progressive increase of the distance between the reactants (adsorbed H and O atoms) as the reaction proceeds stabilizes the initial state and therefore plays a key role in stopping the reaction in the middle of the segments. This leads to the observed comblike propagation of the reaction front.

Second Reaction Step. In the second reaction step, at $T \leq$ 263 K the segmentation of the surface gives rise to a very peculiar final oxygen nanopatterning (see Figure 6). In this step, the remaining oxygen atoms, arranged in a zigzag pattern after the first reaction step, are reacted off. The reaction starts homogeneously from the now enlarged RVs. Initially, this reaction proceeds quickly, but then it slows down markedly so that some oxygen atoms remain on the segments even after 3 h of H_2 exposure (~100 L). Locally, the number of remaining O atoms is almost constant (Figure 6a) so that a pattern forms which is quite regular at the nanoscale. In large-scale images, however, more and less reacted segments are present as well (Figure 6b). The average number of oxygen atoms that remain on the segments was found to depend on the temperature, with more residual O atoms at lower reaction temperatures. To understand whether the pattern formation is due to a particularly stable configuration when a fixed number of zigzag O atoms remains on the segments or due to a limitation in the propagation of the reaction, we prepared a surface consisting of segments with varying lengths[23] and monitored the reaction. It turned out that the length of the reacted part of the segment is rather constant regardless of the overall segment length. This means that the resulting pattern reflects the limited propagation length of the reaction from the RV, rather than a higher stability of the final structure.

The DFT calculations confirm that the reaction starts at the ends of the segments. We again use the OH formation energy as a descriptor for the reaction probability. The OH formation energy at the end of the zigzag segment is −0.56 eV compared to −0.02 eV in the middle of a zigzag segment, indicating that the oxygen atom is more weakly bound and more reactive at the end of a segment than in the center.

Next, we compared the OH formation energies as the reaction proceeds on a long segment (8 Rh atoms) with those on a short segment (4 Rh atoms). Oxygen atoms have been subsequently removed from one side of the segment. It turned out that the OH formation energies depend only on the number of removed oxygen atoms (i.e., the length of the reacted segment) and not on the total length of the segment. The calculated OH formation energies are −0.56, −0.16, and −0.12 eV for hydrogenation of the first, second, and third oxygen atom in the zigzag chain, respectively, being identical for the long and the short Rh segments. The larger OH formation energy on the outermost oxygen atom can again be related to the weaker binding of the oxygen and indicates that this atom is reacted off faster than the remaining oxygen atoms. Once the first oxygen atom has been removed, the OH formation energies stay almost constant. The reaction speed should therefore depend only on the temperature. This correlates with the experimental observation that, after 3 h of H_2 exposure, the average number of oxygen atoms remaining on the segment decreases when the temperature is increased.

Conclusions

We have shown that on the 1D (10 × 2) surface oxide the local topology of the surface plays a fundamental role in the propagation of the water formation reaction. The local segmentation and adsorbate-induced first-layer registry shift is determined by the lattice expansion in the Rh segments. This peculiar surface arrangement and the lattice relaxation during the propagation of the reaction determine the initial geometry for the next reacting O and H atoms and, consequently, the barriers for the OH formation reactions, and is, in this sense, directly responsible for the observed comblike shape of the reaction front.

The overall reaction leads to a sequence of peculiar features at the nanoscale, starting from a nanostructured surface with one-dimensional oxide segments as obtained by the oxidation process. First, during the reduction of the oxide, the specific geometrical configuration at the atomic level governs the reaction, inducing a comblike reaction front that reflects the nanostructuring of the initial surface. Second, a regular low-coverage pattern of residual oxygen atoms adsorbed on metal segments arises after the second reaction step. In this last step, the segmentation plays a crucial role in the nucleation of the reaction. The better aligned the RVs are, the more monodisperse

(23) Starting from a well-ordered (10 × 2), we reacted off the structure at 293 K so that clean segments of various lengths are created. When the surface is slightly re-oxidized (2 L) at low temperature (223 K) and flashed to higher T (~293 K), the segments become covered by oxygen atoms in threefold sites, ordered in a zigzag fashion, without modifying the underlying segment structure.

is the length of the residual oxygen atom chains since the reaction propagation length from the ends of the segments depends only on the temperature and not on the total segment extension.

Since the (10 × 2) structure on Rh(110) is very similar to other 1D surface oxides on stepped rhodium and on Pt(110), our results will also be relevant for reactions on these surfaces. More generally, on the basis of our findings, a progressive variation of the reaction barrier is to be expected for any system where the local geometry around the reactants changes continuously as a consequence of the substrate lattice expansion they induce. This variation, which can be small when moving from one atom to the next one, can nevertheless influence in a remarkable way the overall mechanism of the reaction, which can become as peculiar as in the case we studied, where a comblike path was observed for the reaction front.

Moreover, the observed formation of patterned O distributions might give rise to the formation of specific active sites at the steps of catalysts, which can be used, for example, for partial oxidation reactions of large organic molecules. The observed pattern represents a regular array of sites that provide a topological configuration of the substrate in which the molecules can fit close to periodically distributed oxygen islands.

Acknowledgment. We acknowledge financial support by Fondazione CRTrieste, by Sincrotrone Trieste S.C.p.A., and by the Austrian Science Fund (FWF).

JA808100F